Available online at www.sciencedirect.com
SCIENCE DIRECT®
Thermochimica Acta 419 (2004) 135–141
thermochimica acta
www.elsevier.com/locate/tca

Heat capacity, thermal conductivity, and thermal expansion of barium titanate-based ceramics

Yi He*

Assembly Materials Characterization Laboratory, Intel Corporation, CH5-232, 5000 W. Chandler Blvd., Chandler, AZ 85226-3699, USA

Received 23 October 2003; received in revised form 19 February 2004; accepted 20 February 2004

Abstract

Barium titanate ($BaTiO_3$)-based ceramics have been used widely as dielectric layers in manufacturing multilayer ceramic capacitors (MLCCs) in the electronics industry. In this study, the heat capacities of two different $BaTiO_3$-based ceramic materials were determined as a function of temperature using differential scanning calorimetry (DSC). The densities of these materials were measured at room temperature using Archimedes' principle. Using these experimental values, the thermal diffusivity and thermal conductivity of each material were determined at room temperature with a hot disk sensor, which is a transient technique for rapid thermal conductivity measurement. Finally, the linear coefficients of thermal expansion of these materials were determined using thermomechanical analysis (TMA) from −50 to 250 °C. All these data are useful in modeling the stress and the reliability performance of these chip capacitors under various conditions.

Keywords: $BaTiO_3$; Heat capacity; Thermal conductivity; Thermal expansion; Multilayer ceramic capacitor (MLCC)

1. Introduction

Barium titanate has two structural polymorphous forms at ambient conditions: one is the ferroelectric perovskite phase (p-$BaTiO_3$), and the other is the hexagonal modification, which will not be discussed in this study [1]. Above approximately 120 °C, p-$BaTiO_3$ has a cubic structure and is paraelectric, or non-polar. When the temperature decreases to below 120 °C, spontaneous polarization occurs and the crystal goes through a phase transition to a ferroelectric state [2]. In this process, the cubic crystalline structure, which is stable at $T_c > 120\,^{\circ}C$, is distorted and becomes tetragonal with a c/a ratio of 1.01 at room temperature [1,3,4]. This transition is generally considered to be a first order displacive transition, although theoretical calculations from first principles suggested that it may be better described as an order–disorder transition, which is a second-order transition [5]. A second transition in p-$BaTiO_3$ takes place near 0 °C (±5 °C), below which the crystal remains ferroelectric but the structure becomes orthorhombic [1,6]. Below −80 °C, a third phase transition occurs, and the crystal symmetry becomes rhombohedral [7–10].

Ferroelectric p-$BaTiO_3$ is one of the most extensively studied ferroelectric perovskite materials with many actual and potential applications. $BaTiO_3$-based ceramics are widely used in the electronics industry. One of the most important applications of these materials is as dielectric layers in the multilayer ceramic capacitors (MLCCs), as illustrated in Fig. 1. This is because high dielectric constant of several thousands can be obtained in $BaTiO_3$ near or below its Curie temperature T_c (~120 °C) [11–13]. Along the a-axis, the dielectric constant can be as high as 5000 near room temperature, but it is only about 250 along the c-axis [14]. However, to meet the MLCC application specifications, the temperature dependence of the dielectric constant must be well controlled so that the MLCC will not show dielectric degradation over the application temperature range. For example, the conventional X7R specification set by the Electronic Industries Association requires that the maximum allowed capacitance variation between −55 and 125 °C is ±15% with respect to the room temperature (25 °C) value [15]. To meet such requirements, dopants, such as rare earth elements and their oxides, which can reduce the strong temperature dependence of the dielectric constant near the

---

[*] Tel.: +1-4805523154; fax: +1-4805545241.
E-mail address: yi.he@intel.com (Y. He).

0040-6031/$ – see front matter © 2004 Elsevier B.V. All rights reserved.
doi:10.1016/j.tca.2004.02.008

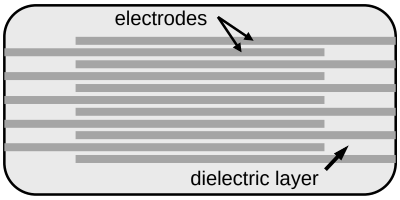

Fig. 1. Illustration of a multilayer ceramic capacitor (MLCC).

phase transitions, are typically added to $BaTiO_3$ to control the microstructure and the grain size [16–20].

MLCCs are an inseparable part of every integrated circuit. The growth of the MLCC market is proportional to the growth of the IC chip production [21]. In 2000, the annual production of MLCCs had exceeded 100 billion [22]. Currently, most of these chip capacitors are surface-mounted on the IC package substrate. It was predicted that by 2005, 40% of these chip capacitors would be incorporated in the substrate through interconnection technology [21].

As semiconductor device size continues to decrease, a key challenge facing electronic packaging is thermal management. The heat generated by the silicon chip will heat up the surrounding components, and it needs to be effectively dissipated to increase device reliability and service life. For this reason, the thermomechanical properties and the thermal transport properties of the MLCC materials need to be characterized for package reliability assessment. For example, when the chip capacitors are embedded in a substrate, the mismatch of the coefficient of thermal expansion (CTE) between the MLCC and the surrounding material (substrate) can cause cracks and delamination during temperature cycling, leading to catastrophic failure.

The purpose of this study is to characterize the heat capacities (C_p), the thermal conductivities (K), and the coefficients of thermal expansion (α) of two different dopant-modified $BaTiO_3$ ceramic materials for potential MLCC applications. These results are important for modeling package reliability performance. In addition, we have also measured the densities of these materials, which are needed in determining the thermal transport properties (thermal conductivity and thermal diffusivity) of these materials.

2. Experimental

2.1. Materials

$BaTiO_3$-based ceramics were manufactured by two different suppliers. The exact chemistry of these materials and the processing conditions are highly proprietary and will not be discussed here. The materials were manufactured from powders using a high temperature sintering technique. The samples used in this study were in a thin square plate form. The typical dimensions are 37 mm × 37 mm × 2.4 mm for samples provided by suppliers A; and 35 mm × 35 mm × 1.4 mm for samples obtained from supplier B.

2.2. Density

The density was measured using Archimedes' principle. Pure de-ionized water was used as the immersion liquid. The density ρ of the sample can be calculated using the following equation:

$$\rho = \frac{m_1 \rho_L}{m_1 - m_2}, \tag{1}$$

where m_1 is the sample weight measured in air, m_2 is the sample weight measured in water, and ρ_L is the density of pure water, which is 0.99821 g/cm^3 at 20 °C [23].

2.3. Heat capacity

Differential scanning calorimetry (DSC) was used to determine the heat capacity of the $BaTiO_3$-based ceramics. The principle of C_p measurement using DSC has been described elsewhere [24,25]. A TA Instruments 2920 modulated DSC operated in the standard mode was used for the heat capacity measurement. A sapphire sample (61.37 mg) was used as the C_p standard. The typical thermal program used for the C_p measurement was:

1. isothermally held at −20 °C for 5 min;
2. ramp at 5 °C/min to 200 °C;
3. isothermally held at 200 °C for 3 min.

To start with the heat capacity measurement, a baseline heat flow curve was first measured with empty aluminum pans. Then, a sapphire standard was placed in the sample pan and the heat flow curve was measured again using the same set of DSC pans. Finally, the heat flow curve of the sample was measured using the same DSC sample pan. The specific heat of the material can then be calculated as [24,25]

$$C_{p1} = \frac{m_2 y_1}{m_1 y_2} C_{p2}, \tag{2}$$

where C_{p1} and C_{p2} are the heat capacity of the sample and the sapphire standard, m_1 and m_2 are the sample mass and the mass of the sapphire standard, and y_1 and y_2 are the net heat flow of the sample and the sapphire, respectively.

Besides the conventional way of measuring C_p as discussed above, a temperature modulated DSC (TMDSC) technique was also used for C_p measurement [26]. TMDSC experiments were conducted from −20 to 200 °C at an underlying heating rate of 3 °C/min. The amplitude of temperature modulation is 0.8 °C, and the period is 100 s. Again, a heat capacity constant calibration was performed using a sapphire standard. After calibration, the measured room temperature C_p of sapphire is within 0.2% of the published value [27].

2.4. Thermal conductivity and thermal diffusivity

Thermal conductivity and thermal diffusivity measurements were conducted using the hot disk technique, which is a transient plane source technique for rapid thermal conductivity measurement [28–31]. The principle of thermal conductivity measurement using the hot disk sensor has been discussed before [29,32,33]. During a hot disk measurement, the hot disk sensor, which is made of a double spiral of nickel wire, is sandwiched between two halves of a sample. A small electric current is supplied to the sensor. The sensor serves as a heat source and as a temperature monitor. It can be shown that the temperature change of the sensor surface, $\Delta\bar{T}$, which can be determined through the resistance measurement, is highly dependent on the thermal transport properties of the surrounding material [29,32,33]:

$$\Delta\bar{T}(\tau) = \frac{P_o}{\pi^{3/2}aK}D(\tau), \tag{3}$$

where P_o is the output power to the sensor, a is the sensor radius, and K is the thermal conductivity of the surrounding material. A dimensionless parameter $\tau = \sqrt{\kappa t}/a$ is called the characteristic time ratio, where κ is the thermal diffusivity of the sample, and t is the measurement time. $D(\tau)$ is a rather complicated function, but can be evaluated numerically to five or six significant figures. If one knows the relationship between t and τ, one can plot $\Delta\bar{T}$ as a function of $D(\tau)$, and a straight line should be obtained. Thermal conductivity can be calculated from the slope of this line. However, the proper value of τ is generally unknown, but it can be determined through a series of optimization processes. In practice, we can measure the density and the specific heat separately, as discussed above. Once ρ and C_p are known, there is only one independent parameter between K and κ since $K = \rho C_p \kappa$. Therefore, both thermal conductivity and thermal diffusivity of the sample can be determined accurately by measuring the average sensor temperature increase as a function of measurement time.

Normally, hot disk measurements are carried out on relatively thick samples (i.e., sample thickness: $>\sqrt{4\kappa t}$) [34]. In the case when only thin slab samples are available, one can still perform the hot disk measurement by insulating the two outer surfaces of the two halves of the sample. Under such configuration, the function $D(\tau)$ in Eq. (3) needs to be modified to include the contribution of all image sources. Mathematically, these image sources are needed to satisfy the physical condition that no net heat can flow across the two outer surfaces [35,36].

In this study, we used a thin slab software module provided with the hot disk tool to perform thermal conductivity measurement of $BaTiO_3$ ceramics [35]. The measurement time was kept at 2.5 s, and the output power to the hot disk sensor was 1 W. The sensor radius is 3.200 mm. At least six measurements were performed for each material to ensure the repeatability of the measurement results.

2.5. Thermal expansion

Linear CTE of $BaTiO_3$ ceramics was measured from −50 to 200 °C at a heating rate of 5 °C/min using a Perkin-Elmer TMA7 system. Although the thermal expansion of single crystalline ferroelectric $BaTiO_3$ is anisotropic [7], it is expected to be isotropic for polycrystalline materials studied in this work. To verify this, thermal expansion coefficients were measured along the *X*-, the *Y*-, and the *Z*-directions; where the *X*-direction is arbitrarily defined as one of the in-plane direction along one edge of the ceramic plate, *Y* the other in-plane direction perpendicular to *X*, and *Z* is along the direction perpendicular to the *XY*-plane. The typical sample length along the *X*-direction is about 10 mm. Along the *Y*-direction, the typical length is about 5 mm. For thermomechanical analysis (TMA) measurement along the *Z*-direction, two or three specimens were stacked together for improved measurement sensitivity. In that case, the sample length along the *Z*-direction is between 4 and 6 mm. For each experiment, three heating scans and two cooling scans were conducted during the experiment. The linear CTE along each direction was calculated based on TMA results.

3. Results and discussion

3.1. Density

Using Archimedes' principle, the average density of the $BaTiO_3$ ceramic material from supplier A was determined to be $5.84 \pm 0.01\,g/cm^3$, where the error is one standard deviation. This value was obtained using three samples and each sample was measured twice. Similar measurements were preformed on three $BaTiO_3$ samples from supplier B, and the result was $\rho = 5.94 \pm 0.02\,g/cm^3$. The difference in density between these two $BaTiO_3$ ceramics can be attributed to the effect of different dopants in these materials. The density results are summarized in Table 1.

3.2. Heat capacity

Fig. 2 shows the typical DSC curves obtained in a conventional heat capacity measurement on a $BaTiO_3$ sample

Table 1
Density, specific heat, thermal conductivity, thermal diffusivity, and coefficient of thermal expansion of two $BaTiO_3$-based ceramic materials determined at room temperature

Material	ρ (g/cm^3)	C_p (J/(g K))	K (W/(m K))	κ (mm^2/s)	α_1 ($\times10^{-6}$ K^{-1})	α_2 ($\times10^{-6}$ K^{-1})
Supplier A	5.84 ± 0.01	0.434 ± 0.004	2.61 ± 0.02	1.03 ± 0.01	6.17	11.29
Supplier B	5.94 ± 0.02	0.406 ± 0.008	2.85 ± 0.04	1.18 ± 0.02	6.01	11.39

For both materials, the CTE1 (α_1) was calculated between 0 and 50 °C, whereas the CTE2 (α_2) was calculated between 150 and 200 °C. The error listed in the table represents one standard deviation.

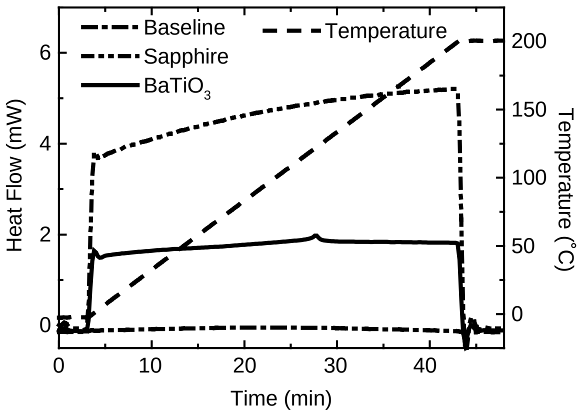

Fig. 2. DSC heat flow curves for the empty pan baseline, the sapphire standard and the $BaTiO_3$ from supplier A.

from supplier A. The heat flow curves for the empty pan baseline, the sapphire standard, and the $BaTiO_3$ sample are plotted together. A small endothermic peak near 120 °C is clearly visible, which is related to the ferroelectric transition.

Fig. 3 shows the heat capacity curves of $BaTiO_3$ from supplier A obtained during two conventional DSC experiments and one TMDSC measurement. All three curves showed a small peak near 120 °C, which corresponds to the ferroelectric transition. The other transition that supposedly occurs near 5 °C in pure $BaTiO_3$ was not detected in these two materials. At room temperature (20 °C), the average C_p of the material from supplier A is 0.434 ± 0.004 J/(g K). This value is consistent with literature data of pure $BaTiO_3$, which has a C_p of 0.439 J/(g K) at 300 K (27 °C) [37]. For $BaTiO_3$ from supplier B, the average room temperature C_p is 0.406 ± 0.008 J/(g K). Therefore, the volumetric specific heat (ρC_p) is 2.5324×10^6 J/(m^3 K) for $BaTiO_3$ from supplier A and 2.411×10^6 J/(m^3 K) for $BaTiO_3$ from supplier B. These values will be used to calculate thermal conductivity and thermal diffusivity when analyzing the results from the hot disk measurement.

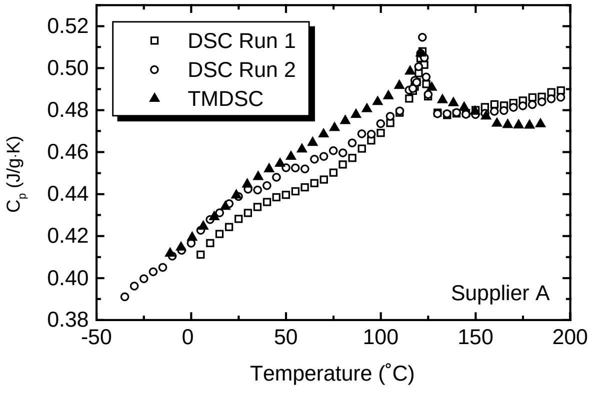

Fig. 3. Heat capacity of $BaTiO_3$ ceramic material from supplier A obtained from conventional DSC and TMDSC experiments.

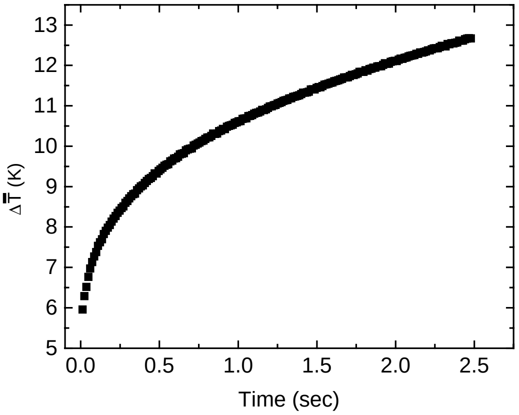

Fig. 4. Average increase in sensor temperature as a function of measurement time during a typical hot disk measurement of $BaTiO_3$ ceramics from supplier A. The power input to the sensor was 1 W.

3.3. Thermal conductivity and thermal diffusivity

Fig. 4 represents the average temperature increase of the sensor, $\Delta\bar{T}$, as a function of time during a typical hot disk measurement for $BaTiO_3$ ceramics from supplier A. The initial jump in $\Delta\bar{T}$ is due to the contact thermal resistance and the resistance of the polyimide insulation film on the hot disk sensor. The effect of contact resistance can be corrected in the subsequent optimization process [34]. Based on the $\Delta\bar{T}$ versus time curve, one can calculate $\Delta\bar{T}$ as a function of $D(\tau)$, as discussed earlier. Fig. 5 plots $\Delta\bar{T}$ versus $D(\tau)$, from which the bulk thermal conductivity of this $BaTiO_3$ is determined to be 2.65 W/(m K), and the thermal diffusivity is 1.05 mm^2/s. Based on eight such measurements, the average thermal conductivity is 2.61 W/(m K), with a standard deviation of 0.02 W/(m K). The corresponding thermal diffusivity is 1.03 ± 0.01 mm^2/s. The results are listed in Table 1.

Similar experiments were performed on $BaTiO_3$ ceramics from supplier B. Based on eight measurements, the thermal

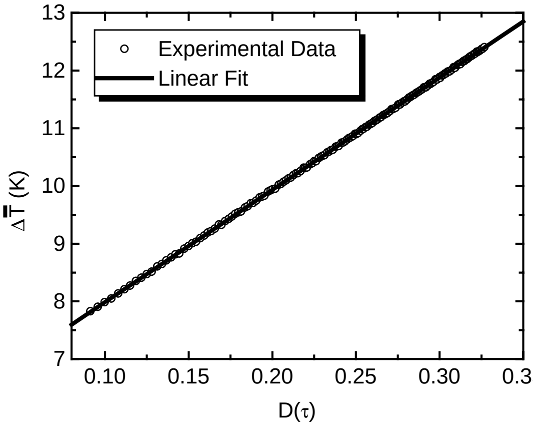

Fig. 5. Plot of $\Delta\bar{T}$ as a function of $D(\tau)$ as deduced from the $\Delta\bar{T}$ vs. time curve shown in Fig. 4. Data points 12–180 were used in the calculation. A linear fit of the experimental data has a correlation coefficient of $R = 0.99998$.

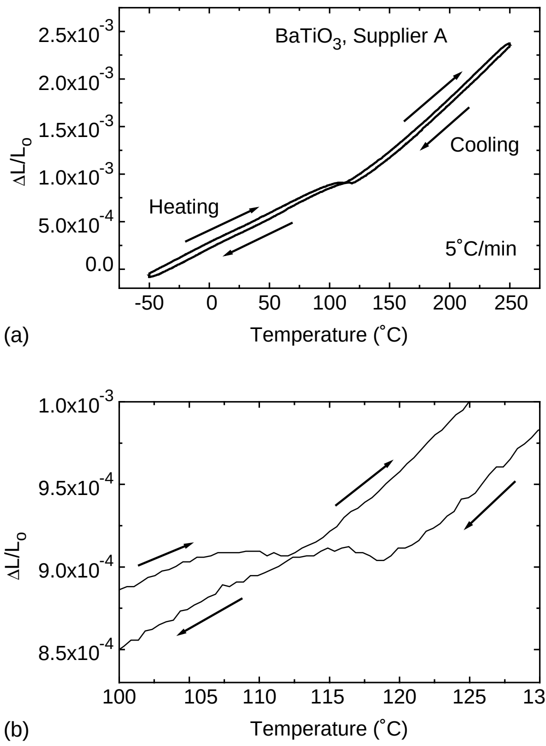

Fig. 6. (a) Relative change in sample length along the *X*-direction as a function of temperature obtained by TMA. Both heating and cooling ramps are included. (b) Enlarged TMA curves over the ferroelectric transition temperature range.

conductivity was determined to be 2.85 ± 0.04 W/(m K), and the thermal diffusivity was 1.18 ± 0.02 mm^2/s, as shown in Table 1.

Literature data on room temperature thermal conductivity of $BaTiO_3$ ranged from 1.3 to 6 W/(m K) [38]. The main source of variation can be attributed to different manufacturing procedures used to prepare these samples, different dopants added in these materials, and different techniques used for thermal conductivity measurement. Our results are within the range of the reported data.

3.4. Thermal expansion

For both materials from suppliers A and B, the thermal expansion along the *X*-direction was measured first. For each TMA experiment, multiple heating and cooling scans were carried out. The first heating scan is designed to remove or reduce possible stress in the sample induced during the manufacturing process. Results showed that in our samples, the strain effect is negligible. Fig. 6(a) plots the relative change in sample length ($\Delta L/L_0$) along the *X*-direction as a function of temperature for a typical sample from supplier A. Both the second heating and the second cooling ramps are included in the plot. Based on Fig. 6(a), we noticed that $\Delta L/L_0$ versus temperature curve has a small plateau near about 120 °C, which is associated with the ferroelectric transition, as observed a long time ago [1]. The width of this transition plateau depends on the microstructure of the material. Fig. 6(b) is an enlarged view of the TMA curves over the narrow transition range. There is a small "thermal hysteresis" between the heating and the cooling curves. Based on Fig. 6(b), it can be seen that on heating, the tetragonal to cubic phase transition starts at approximately 106 °C; whereas on cooling, the reverse transition occurs near 119 °C. Repeated measurements revealed that both heating and cooling ramps are very repeatable. TMA measurements along the *X*-direction of $BaTiO_3$ from supplier B showed similar results, as shown in Fig. 7. The other transition near 0 ± 5 °C, which was observed in pure $BaTiO_3$ [1], was not detected in these two materials. It is likely that the added dopants and modified microstructure in these two $BaTiO_3$ ceramics extended the stability range of the tetragonal phase, or the dimensional change during this transition becomes too small to be detected by TMA.

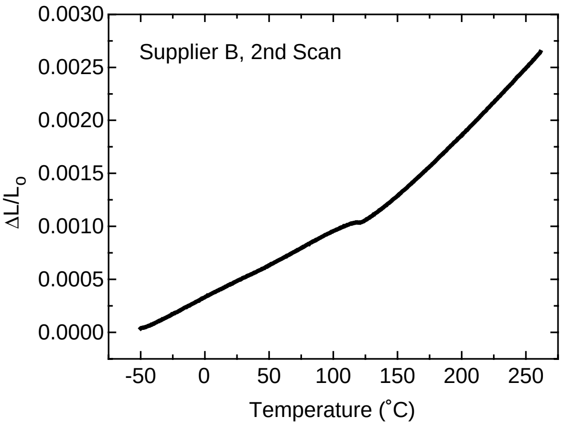

Fig. 7. Relative increase in sample length during the second heating scan for a $BaTiO_3$ sample from supplier B (*X*-direction).

The second heating scan, such as the one shown in Fig. 7, was used to calculate the CTE. Careful examination of the thermal expansion curve revealed that within the narrow temperature range of the ferroelectric transition, the thermal expansion becomes negative, as shown in Fig. 8. Negative

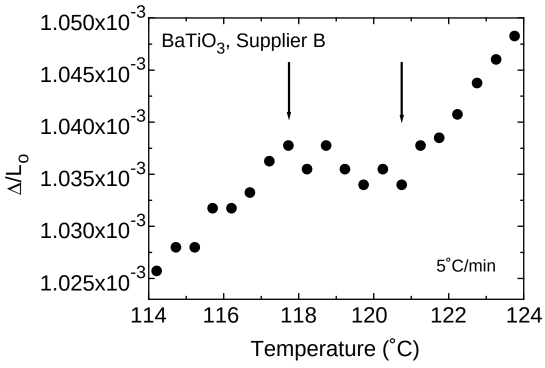

Fig. 8. An enlarged TMA plot focusing only on the ferroelectric transition region revealed that over the narrow temperature range of the transition region (as indicated by the arrows), this $BaTiO_3$-based ceramic material displays a small thermal contraction, indicating that the thermal expansion becomes negative. The sample was the same as used to obtain Fig. 7.

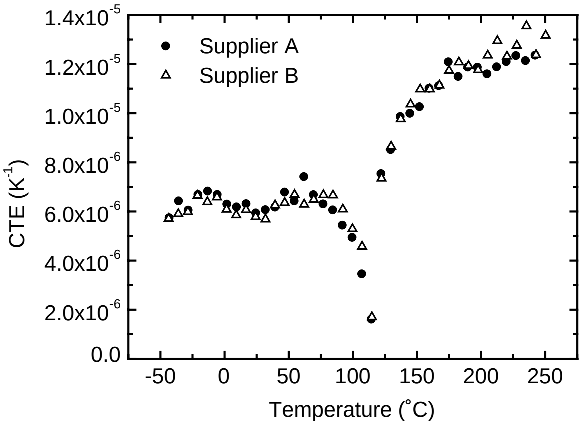

Fig. 9. Calculated CTE along the *X*-direction as a function of temperature for $BaTiO_3$ from both suppliers. Near the ferroelectric transition temperature, CTE approaches zero or even slightly negative (see Fig. 8).

thermal expansion has been known to exist in $BaTiO_3$, $PbTiO_3$ and other ABO_3 types of perovskite oxides [39]. The negative thermal expansion near Curie temperature has also been observed in crystalline triglycine sulfate [40].

Fig. 9 shows the calculated coefficients of thermal expansion along the *X*-direction for both materials. When calculated between 0 and 50 °C, both materials have a room temperature CTE of about $6 \times 10^{-6}\,K^{-1}$. When calculated between 150 and 200 °C, the average CTE at 175 °C of both materials is about $(11.3–11.4) \times 10^{-6}\,K^{-1}$, as listed in Table 1. When the temperature approaches the ferroelectric transition temperature, the CTE of both materials decreases rather sharply and it even becomes negative for a short temperature range, as shown in Fig. 8. This is because near the ferroelectric transition, the displacive nature of the transition causes the crystalline lattice to contract. Based on Fig. 8, we estimated that the CTE over the ferroelectric transition range for sample B is $-1.2 \times 10^{-6}\,K^{-1}$. Such negative expansion upon heating over the ferroelectric transition range has been detected before using both X-ray diffraction and dilatometric measurements [41].

Additional TMA measurements were performed on both materials along the *Y*- and the *Z*-directions. Within experimental error, the thermal expansion behavior along both the *Y*- and the *Z*-directions are the same as the one along the *X*-direction, as shown in Fig. 10, where the relative change in sample length along all three directions were plotted together for the material obtained from supplier A. Thus, TMA results suggested that for these polycrystalline materials, the thermal expansion is very much isotropic. The thermal contraction upon heating to ferroelectric transition region is detected in all three directions.

TMA analysis showed that below ferroelectric transition temperature, the linear CTEs for both $BaTiO_3$ ceramics are around $6 \times 10^{-6}\,K^{-1}$, and the CTEs quickly increase to above $10 \times 10^{-6}\,K^{-1}$ once $T > T_c$. On the other hand, for organic substrate materials typically used in microelectronics industry, the typical CTE within the substrate plane is $(12–18) \times 10^{-6}\,K^{-1}$, and the CTE perpendicular to the plane is typically $(25–50) \times 10^{-6}\,K^{-1}$. Therefore, there is a noticeable CTE mismatch between the substrate and the MLCCs over the entire temperature range between −50 and 250 °C. When chip capacitors are embedded in the substrate, CTE mismatch becomes a serious reliability concern because it causes thermal stresses in the package during temperature cycling, which can lead to cracking and delamination within the substrate, resulting in package failure. Unless this issue is resolved, it is preferred to surface-mount the MLCCs rather than to embed them in the substrate.

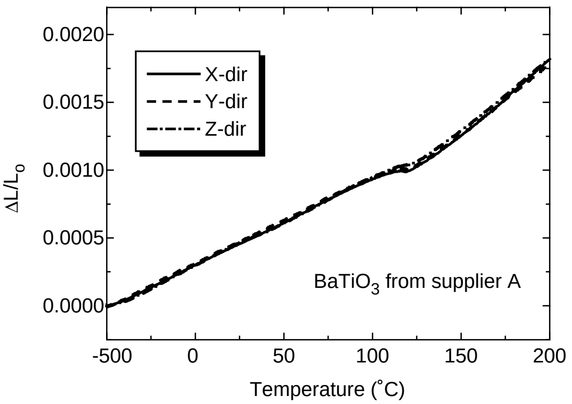

Fig. 10. Relative change in sample length along the *X*-, the *Y*-, and the *Z*-directions for $BaTiO_3$ from supplier A.

4. Conclusions

In conclusion, we have characterized the density, heat capacity, thermal diffusivity, thermal conductivity and thermal expansion of two different $BaTiO_3$-based ferroelectric ceramic materials with potential applications as a dielectric material for MLCCs in the microelectronics industry.

Using Archimedes' principle, the densities of these materials were determined to be 5.84 and 5.94 g/cm^3, respectively. DSC experiments showed that the heat capacities were in the range of 0.41–0.43 J/(g K). Density and heat capacity data were used in the hot disk experiment to determine the thermal diffusivity and the thermal conductivity. The results showed that the thermal diffusivities were 1.0 and 1.2 mm^2/s and the thermal conductivities were 2.6 and 2.85 W/(m K), respectively, for the samples obtained from supplier A and B. TMA measurements showed that both materials are isotropic and have a linear CTE of about $6 \times 10^{-6}\,K^{-1}$ near room temperature. Above the ferroelectric transition temperature, CTE of both materials increases to above $10 \times 10^{-6}\,K^{-1}$. Over the entire temperature range of our measurement, these values are significantly smaller than the typical CTE of an organic substrate material. This CTE mismatch is a major reliability concern for embedded chip capacitors. Our experimental data are very useful to model the heat dissipation through the capacitors and the thermal stress induced in the capacitor/substrate interface due to CTE mismatch.

Acknowledgements

I am grateful to Dr. Cengiz A. Palanduz for technical discussions, and Mr. Alan Overson for experimental assistance. Careful review of the manuscript by Drs. Tom Miller and John Briscoe is highly appreciated.

References

[1] A. von Hippel, Ferroelectricity, domain structure, and phase transitions of barium titanate, Rev. Mod. Phys. 22 (1950) 221–237.

[2] For high-purity $BaTiO_3$, the curie temperature is 130 °C, see, for example, T. Mitsui, I. Tatsuzaki, E. Nakamura, An Introduction to the Physics of Ferroelectrics, Gordon and Breach, New York, 1974.

[3] H.D. Megaw, Proc. Phys. Soc. (Lond.) 58 (1946) 133;
H.D. Megaw, Trans. Faraday Soc. 42A (1946) 224;
H.D. Megaw, Proc. R. Soc. 189 (1947) 261.

[4] B.C. Frazer, H.R. Danner, R. Pepinsky, Single-crystal neutron analysis of tetragonal $BaTiO_3$, Phys. Rev. 100 (1955) 745–746.

[5] W. Zhong, D. Vanderbilt, K.M. Rabe, Phase transition in $BaTiO_3$ from first principles, Phys. Rev. Lett. 73 (1995) 1861–1864.

[6] G. Shirane, H. Hanner, R. Pepinsky, Neutron diffraction study of orthorhombic $BaTiO_3$, Phys. Rev. 105 (1957) 856–860.

[7] H.F. Kay, P. Vousden, Phil. Mag. 40 (1949) 1019.

[8] P.W. Forsbergh, Domain structures and phase transitions in barium titanate, Phys. Rev. 76 (1949) 1187–1201.

[9] F. Jona, R. Pepinsky, Symmetry of the low-temperature phase of $BaTiO_3$, Phys. Rev. 105 (1957) 861–864.

[10] E. Sawaguchi, M.L. Charters, Symmetry of the low-temperature phase of barium titanate, Phys. Rev. 117 (1960) 465–469.

[11] Y. Sakabe, Multilayer ceramic capacitors, Curr. Opin. Solid State Mater. Sci. 2 (1997) 584–587.

[12] A.J. Moulson, J.M. Herbert, Electroceramics: Materials, Properties and Applications, Chapman & Hall, London, 1990.

[13] L. Shepperd, Progress continues in capacitor technology, Am. Ceram. Soc. Bull. 72 (3) (1993) 45–47.

[14] W.J. Merz, The electric and optical behavior of $BaTiO_3$ single-domain crystals, Phys. Rev. 76 (1949) 1221–1225.

[15] See, for example, Technical Brochure from Novacap, http://www.novacap.com/tech_brochure.pdf.

[16] B. Zaffe, W.R. Cook, H. Jaffe, Piezoelectronic Ceramics in Nonmetallic Solid: Series of Monographs No. 3, Academic Press, London, 1971, p. 53.

[17] Y. Park, Y.H. Kim, The dielectric temperature characteristic of additives modified barium titanate, J. Mater. Res. 10 (1995) 2770–2776.

[18] A.C. Caballero, J.F. Fernádez, C. Moure, P. Durán, J.L.G. Fierro, Dopant distribution and grain growth control in $BaTiO_3$ ceramics doped with $ZnO–SiO_2–P_2O_5$, J. Eur. Ceram. Soc. 17 (1997) 1223–1230.

[19] Y. Park, H.G. Kim, The microstructure analysis of cerium-modified barium titanate having core–shell structured grains, Ceram. Int. 23 (1997) 329–336.

[20] H. Kishi, N. Kohzu, J. Sugino, H. Ohsato, Y. Iguchi, T. Okuda, The effect of rare-earth (La, Sm, Dy, Ho and Er) and Mg on the microstructure in $BaTiO_3$, J. Eur. Ceram. Soc. 19 (1999) 1043–1046.

[21] B.C.H. Steele, R.E. Newnham, A.G. Evans, Ceramics, composites and intergrowths, Curr. Opin. Solid State Mater. Sci. 2 (1997) 563–565.

[22] N. Setter, R. Waser, Electroceramic materials, Acta Mater. 48 (2000) 151–178.

[23] D.R. Lide (Editor in Chief), CRC Handbook of Chemistry and Physics, 80th ed., CRC Press, Boca Raton, 1999, p. 6-3.

[24] M.J. O'Neill, Anal. Chem. 18 (1966) 1331–1336.

[25] P.J. Haines, F.W. Wilburn, in: P.J. Haines (Ed.), Thermal Methods of Analysis: Principles, Applications and Problems, Blackie Academic and Professional, London, 1995 (Chapter 3).

[26] M. Reading, A. Luget, R. Wilson, Modulated differential scanning calorimetry, Thermochim. Acta 238 (1994) 295–307.

[27] D.A. Ditmars, et al., J. Res. Nat. Bur. Stand., 87 (2) (1985) 159–163 (as quoted by TA Instruments DSC 2920 Operator's Manual, 1995, TA Instruments).

[28] S.E. Gustafsson, E. Karawacki, M.N. Khan, J. Phys. D: Appl. Phys. 12 (1979) 1411–1421.

[29] S.E. Gustafsson, Rev. Sci. Instrum. 62 (1991) 797–804.

[30] S.E. Gustafsson, B. Suleiman, N.S. Saxena, I. ul Haq, High Temp. High Press. 23 (1991) 289–293.

[31] E. Karawacki, B. Suleiman, Meas. Sci. Technol. 2 (1991) 744–750.

[32] V. Bohac, M.K. Gustavsson, L. Kubicar, S.E. Gustafsson, Rev. Sci. Instrum. 71 (2000) 2452–2455.

[33] Y. He, Rapid Thermal conductivity measurement with a hot disk sensor. Part 1. Theoretical considerations, in: Proceedings of the 30th North American Thermal Analysis Society Conference, Pittsburgh, PA, 2002, pp. 499–504.

[34] S.E. Gustafsson, E. Karawacki, M.A. Chohan, J. Phys. D: Appl. Phys. 19 (1986) 727–735.

[35] M. Gustavsson, E. Karawacki, S.E. Gustafsson, Rev. Sci. Instrum. 65 (1994) 3856–3859.

[36] Y. He, submitted for publication.

[37] Y.S. Touloukian, E.H. Buyco (Ed.), Thermophysical Properties of Matter, vol. 5, Specific Heat: Nonmetallic Solids, IFI/Plenum Press, New York, 1970.

[38] Y.S. Touloukian, R.W. Powell, C.Y. Ho, P.G. Klemens, Thermophysical Properties of Matter, vol. 2, Thermal Conductivity: Nonmetallic Solids, IFI/Plenum Press, New York, 1970.

[39] A.W. Sleight, Negative thermal expansion materials, Curr. Opin. Solid State Mater. Sci. 3 (1998) 128–131.

[40] K. Imai, J. Phys. Soc. Jpn. 43 (1977) 1320.

[41] F. Jona, G. Shirane, Ferroelectric Crystals, Pergamon Press, New York, 1962 (Chapter IV).